DOI 10.1007/s11182-023-02952-x
Russian Physics Journal, Vol. 66, No. 4, August, 2023

SYNTHESIS OF TECHNICAL CERAMICS IN A BEAM OF FAST ELECTRONS

S. A. Ghyngazov, I. P. Vasil'ev, V. A. Boltueva, and V. A. Vlasov UDC 666.3.7

Samples of zirconia-toughened alumina are synthesized in a beam of fast electrons. The initial raw material is an 80%Al_2O_3–20%(ZrO_2–3Y_2O_3) *nanopowder. A separate attention is given to processing of the green-density powder mixture and the compacted powder plates. The trays with the powder samples are displaced in the beam incidence plane at a rate of 1 m/s. In the first case, the synthesized material mainly consists of the corundum (78.7%) and zirconia phases. In the second case, the content of corundum in the powder sample is found to be 16%.*

Keywords: zirconia-toughened alumina, fast electrons, synthesis.

INTRODUCTION

Oxide ceramics is the most common natural material. Along with the use of natural oxides mined in different deposits, the engineering industries use ultrapure materials produced by the chemical [1, 2] and plasmochemical [3, 4] methods, by laser evaporation [5] and other processes [6, 7]. A characteristic representative of these materials is alumina most frequently occurring in the nature as corundum. Despite a long history of its application, in the current stage of technological development the interest to alumina is still unfailing. For instance, Yang et al. [8] discuss new unique properties of corundum nanoparticles. A special attention is given to the production of refractory ceramics based on the alumina system [9–11]. There is a well-known application of corundum-based materials in biomedicine [12]. An addition of zirconia into corundum improves the service properties of the abrasive material [13]. The use of this type of ceramics is especially promising for designing macroporous ceramics [14].

Zirconia alumina, belonging to artificial doped zirconia-toughened alumina, is produced by melting aluminum earth in a tilting electric-arc furnace using doping agents of zirconia and baddeleyite concentrate. The resulting molten material is subjected to high-intensity cooling. The production cycle of zirconia alumina is characterized by high sintering temperatures and long process durations. In this connection, it is critical to develop new high-efficiency methods for synthesizing complex-oxide materials within reasonably short production times. A good promise in this field is demonstrated by the radiation-thermal treatment in a high-power beam of fast electrons. Its efficiency has been proven in a large number of studies on synthesizing a variety of complex-oxide compounds in electron beams, such as ferrite synthesis under the conditions of electron beam heating [15–20]. A peculiarity of the cited publications is the use of the radiation-heating temperatures not exceeding the characteristic temperatures of sintering of ceramics of the same compositions. Despite the essentially faster synthesis process, the total production time was still rather long, which also affected the production cost.

In this work, using the synthesis of zirconia-toughened alumina as an example, we demonstrate that high-temperature complex-oxide ceramics can be effectively synthesized within short production times under the conditions of fast-electron-beam heating to the melting temperature of one of the mixture components.

National Research Tomsk Polytechnic University, Tomsk, Russia, e-mail: ghyngazov@tpu.ru; zarkvon@tpu.ru; kostenkova@tpu.ru; vlvitan@tpu.ru. Original article submitted June 6, 2023.

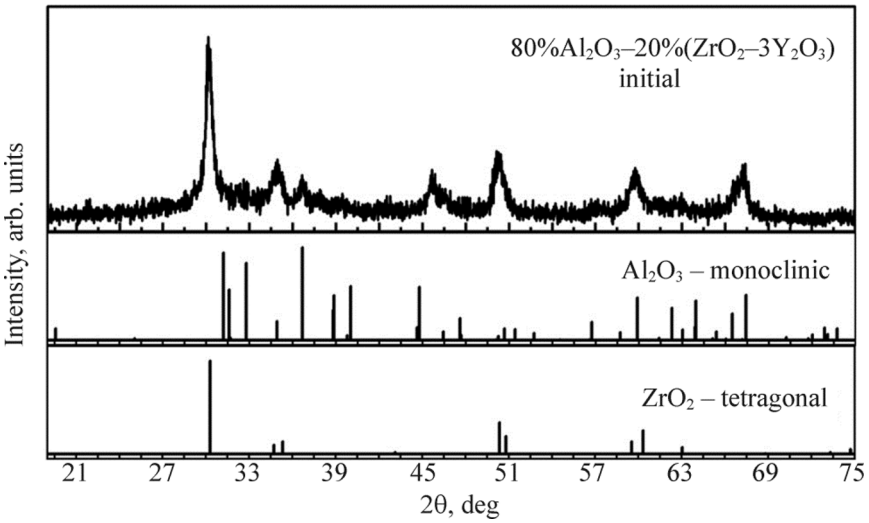

Fig. 1. XRD pattern of the initial $80\%Al_2O_3–20\%(ZrO_2–3Y_2O_3)$ powder.

MATERIALS AND EXPERIMENTAL METHODS

The raw material for the synthesis was a nanopowder of the following composition: $80\%Al_2O_3–20\%(ZrO_2–3Y_2O_3)$, which was manufactured by the plasmochemical process. The powders were irradiated in an electron accelerator (ELV-6 accelerator, a unique research facility at INP SB RAS, Novosibirsk). A beam of fast 2.0 MeV electrons was extracted into the air through an outlet unit containing a system of intermediate evacuation. The beam power was varied by the current-mode control. The power density in the irradiation plane was as high as 28 kW/cm^2. The powder mixture was placed into a massive copper tray. The powder layer thickness was selected according to the condition of a complete electron flux absorption in the bulk of the powder. We examined two powder mixture variants in the irradiated samples. The first method – poring of the powder into the tray, i.e. the powder state was characterized by its green density. The second – the powder was compacted in a special die to form 20×80×3 mm^3 plates that were then placed into the tray. In both cases, the specific powder weight per unit area was 0.9 g/cm^2. This value was chosen based on the condition of a complete absorption of the electron flux as it penetrated into the irradiated volume of the powder sample or the compacted plate. The tray with the samples was displaced in the electron beam incidence plane at a rate of 1 cm/s. Concurrently the beam cross section was also scanned. The scanned region was 5 cm.

An examination by the scanning electron microscopy (SEM) was carried out in a TM-3000 scanning electron microscope (Hitachi, Japan). An X-ray diffraction analysis was performed in an X'TRA powder X-ray diffraction system (ARL, Switzerland).

EXPERIMENTAL RESULTS

Characteristics of initial material. According to the data reported in [3], the $80\%Al_2O_3–20\%(ZrO_2–3Y_2O_3)$ plasmochemical powder consists of flaked nanoparticles combined into large agglomerates. An XRD analysis (Fig. 1) reveals that it contains 19.3% of tetragonal zirconia and 80.7% of alumina.

Irradiation of green-density powder material. After irradiation, very little ceramic material was left in the tray (on the order of a few percent of the initial amount). The nanopowders were carried over from the tray by the air flow used to protect the extraction unit of the accelerator from the products of the irradiated powder decomposition and evaporation. An essential role in this process could have been played by charging of nanoparticles by the electrons, which gave rise to their removal by the air flow. Nevertheless, a small amount of the synthesized material remained in

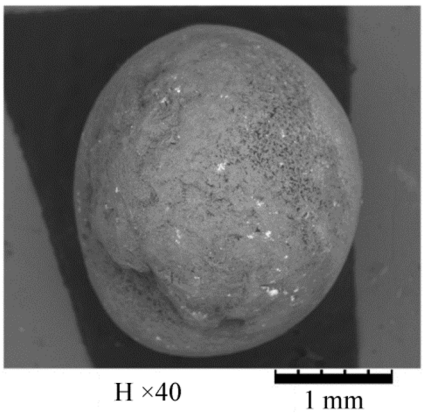

Fig. 2. SEM image of a dropwise synthesis product. General view.

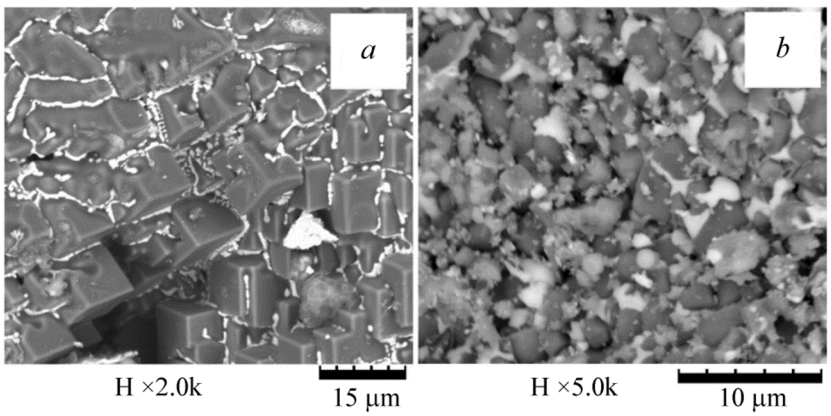

Fig. 3. SEM image of a dropwise synthesis product under high magnification: *a* – surface; *b* – inner part.

the crucible. The resulting product particles have nearly spherical shapes. Figure 2 gives a SEM image of a large particle. Its dropwise shape suggests that at least one component of the powder mixture has melted during heating by fast electrons. Since the melting temperature of Al_2O_3 is noticeably lower than that of ZrO_2, one would reasonably expect that melting of the former oxide did take place.

A detailed SEM image of the product, given in Fig. 1, is presented in Fig. 3*a*. It is evident that the sintered material microstructure mostly consists of a collection of cubic-shape crystals, obviously corundum, with the zirconia inclusions homogeneously distributed along their boundaries. A SEM analysis of the inner regions of the dropwise product (Fig. 3*b*) did not reveal any characteristic ordered structure observed in Fig. 3*a*. The inner part represents a collection of corundum grains, between which there are homogeneously distributed zirconia particles (Fig. 3*b*). A comparison of Figs. 3*a* and *b* demonstrates that the characteristic particle-forming is typical for the molten material surface only.

An XRD analysis demonstrates that the phase composition of the irradiated material has changed (Fig. 4). It should be noted that the content of the tetragonal phase of zirconia remained at the same level (21%), while the alumina has completely transformed into the corundum phase (78.7%). At the same time, new peaks have been revealed, presumably attributed to Zr_5Al_3O (0.4%).

Irradiation of compacted powder samples. After irradiation of the compacted powder sample the powder material volume in the tray was practically the same. The weight loss was as low as 10%. As a result of electron beam

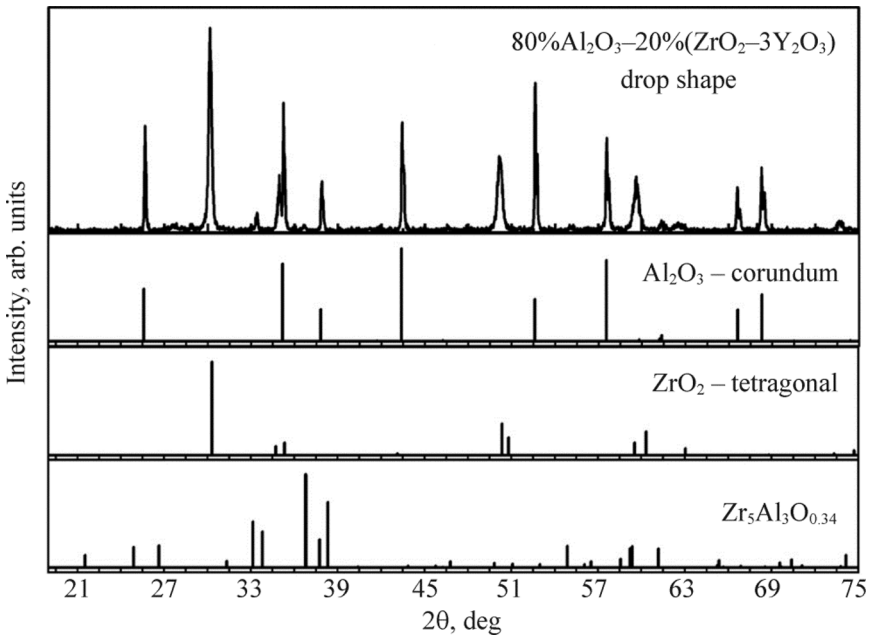

Fig. 4. XRD patterns from the $80\%Al_2O_3–20\%(ZrO_2–3Y_2O_3)$ green-density powder samples irradiated with high-power fast electrons.

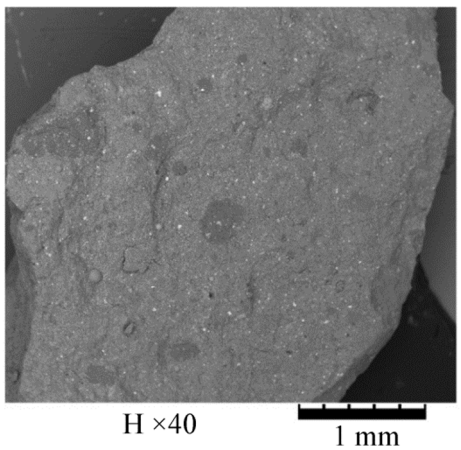

Fig. 5. General view of a compacted powder fragment after its irradiation with fast electrons.

irradiation, the compacted powder sample separated into blocks measuring a few square millimeters (Fig. 5). No macrodroplets were observed to form. At the same time, at higher magnifications one can see numerous spherical microsized formations (Fig. 6). Therefore, it is a stated fact that the formations similar to those presented in Fig. 2 are observed at the microlevel.

An XRD analysis demonstrated that an irradiation of the compacted powder samples resulted in the formation of spherical microinclusions and the noticeable change of the phase composition (Fig. 7). The content of the tetragonal phase has remained at the same level (21%), while alumina is observed to contain new phases, such as corundum (16%), Kappa (16%), Delta (42%), and cubic (1.6%) phases. The formation of new alumina phases different from corundum can be accounted for by the heating that was insufficient to provide a complete transition of the entire volume

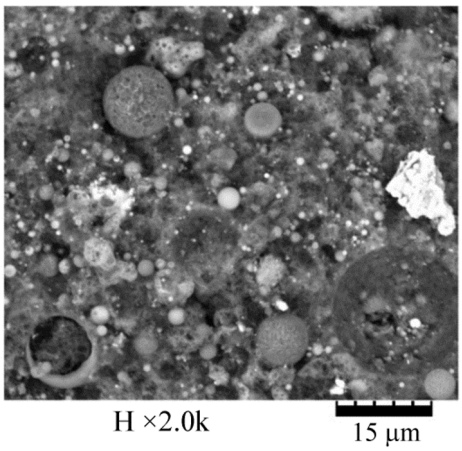

Fig. 6. SEM image of the fragment given in Fig. 5 at higher magnification.

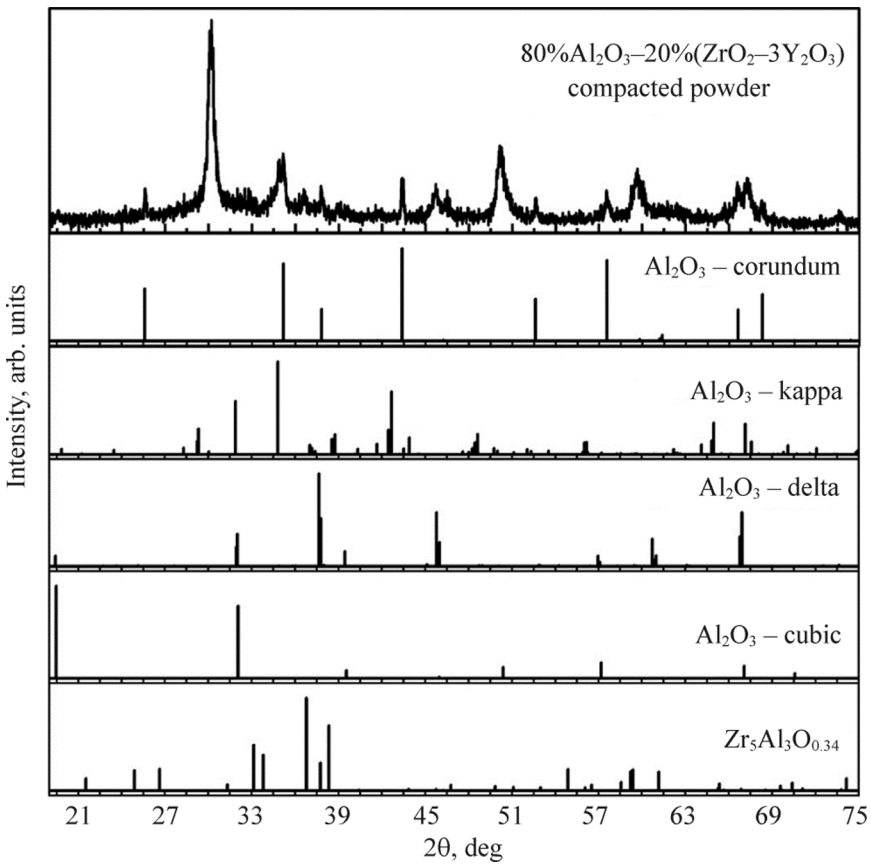

Fig. 7. XRD pattern from a compacted powder sample irradiated with fast electrons.

of alumina into corundum. Due to a high density of the compacted samples, the electron absorption efficiency has decreased compared to that of the green-density samples. Note that part of the electrons penetrated through the compacted samples and was absorbed in the copper tray, heating it.

CONCLUSIONS

Within short time durations (few seconds), zirconium corundum samples have been synthesized in a beam of fast electrons. It has been found out that the microstructure of the synthesized ceramic material strongly depends on the state of the initial powder product prior to its irradiation. If the powder placed into the tray is in the state of green density, the synthesized product has a dropwise shape and consists of a collection of alumina microcrystals, between which there are homogeneously distributed zirconia inclusions. The outer surface of the dropwise formations consists of characteristic cubic alumina microcrystals. The phase composition changes are observed in alumina only. From its monoclinic phase alumina practically entirely transforms into a corundum phase.

When the initial powder is placed into the tray in a compacted state, then at the same irradiation conditions, there is no formation of macrodroplets. The completeness of compacted powder samples is distorted, resulting in the formation of a structure consisting of large blocks. Inside these blocks there are spherical microinclusions, which are likely to result from the synthesis of zirconium corundum. This is indicated by the XRD data demonstrating that in this case no initial monoclinic phase is observed. Instead, there are new phases, such as corundum (16%); Kappa (16%); Delta (42%), and cubic (1.6%) phases.

Therefore, an irradiation of the initial material with a beam of fast electrons makes it possible within short time periods to synthesize zirconia-toughened yttria-stabilized alumina. Importantly, the microstructure and amount of the synthesized products, as well as the irradiation modes could be regulated by varying the density of the initial pwder material.

This work was carried out using financial support from the Russian Science Foundation (project No. 23-79-00014).

REFERENCES

1. R. A. Andrievsky and A. V. Ragulya, Nanostructured Materials [in Russian], Academy, Moscow (2005).
2. A. V. Nikam, B. L. V. Prasad, and A. A. Kulkarni, CrystEngComm, **20**, 5091 (2018). DOI https://doi.org/10.1039/C8CE00487K.
3. A. B. Vorozhtsov, A. S. Zhukov, T. D. Malinovskaya, and V. I. Sachkov, Synthesis of Dispersed Metal Oxide Materials. Book 2. Plasma-chemical method for synthesizing titanium and zirconium oxides, [in Russian], NTL, Tomsk (2014).
4. Z. Sagdoldina, K. Shestakov, M. Yermolenko, M. Kylyshkanov, M. Podoinikov, B. Rakhadilov, and Y. Kambarov, Coatings, **12**, 1658, (2022). DOI https://doi.org/10.3390/coatings12111658.
5. E. György, A. Perez del Pino, A. Datcu, L. Duta, C. Logofatu, I. Iordache, and A. Duta, Ceram. Int., **42 (14)**, 16191 (2016). DOI:10.1016/j.ceramint.2016.07.140.
6. M. Parashar, V. K. Shukla, and R. Singh, J. Mater Sci: Mater Electron., **31**, 3729 (2020). DOI https://doi.org/10.1007/s10854-020-02994-8.
7. V. G. Ilves, V. S. Gaviko, A. M. Murzakaev, S. Yu Sokovnin, M. A. Uimin, and M. G. Zuev, Ceram. Int., **49 (13)**, 21848 (2023). DOI https://doi.org/10.1016/j.ceramint.2023.04.007.
8. H. Yang, B. Wang, H. Zhang, B. Shen, Y. Li, M. Wang, J. Wang, W. Gao, Y. Kang, Lu Li, Y. Dong, J. Li, and Ju Li, Acta Mater., **255**, 119038 (2023). DOI https://doi.org/10.1016/j.actamat.2023.119038.
9. Y. Yang, H. Liu, Z. Wang, Y. Ma, and X. Wang, Ceram. Int., **49 (14)**, 23558 (2023). DOI https://doi.org/10.1016/j.ceramint.2023.04.190.
10. H. Nakaishi, T. Yabutsuka, T. Yao, S. Kitao, M. Seto, Wen-Jauh Chen, Y. Shimonishi, S. Yoshida, and S. Takai, Mater. Chem. Phys., **303**, 127764 (2023). DOI https://doi.org/10.1016/j.matchemphys.2023.127764.
11. Q. Zheng, Y. Li, C. Ma, J. Sun, Y. Gao, and H. Li, J. Eur. Ceram., **43 (8)**, 3788 (2023). DOI https://doi.org/10.1016/j.jeurceramsoc.2023.02.052.

12. A. M. Claro, C. C. Alves, K. S. dos Santos, E. G. da Rocha, M. de Lima Fontes, G. C. Monteiro, G. S. Gonçalves de Carvalho, J. M. Almeida Caiut, A. Moroz, S. J. Lima Ribeiro, and H. S. Barud, J. of Sol-Gel Sci. Technol., **107 (1)**, 83 (2023). DOI 10.1007/s10971-022-05990-y.
13. M. Varga, R. Grundtner, M. Maj, F. Tatzgern, and K.-O. Alessio, Wear, **522**, 204700 (2023). DOI 10.1016/j.wear.2023.204700.
14. O. A. Fouad, M. M. S. Wahsh, G. G. Mohamed, and M. M. El-Dessouky, Mater. Chem. Phys., **301**, 127617 (2023). DOI 10.1016/j.matchemphys.2023.127617.
15. E. N. Lysenko, V. A. Vlasov, E. V. Nikolaev, A. P. Surzhikov, and M. V. Korobeynikov, Mater. Chem. Phys., **302**, 127722 (2023). DOI https://doi.org/10.1016/j.matchemphys.2023.127722.
16. E. Lysenko, V. Vlasov, E. Nikolaev, A. Surzhikov, and S. Ghyngazov, Materials, **16 (2)**, 604 (2023). DOI https://doi.org/10.3390/ma16020604.
17. A. P. Surzhikov, E. V. Nikolaev, E. N. Lysenko, S. A. Nikolaeva, D. Z. Karabekova, and A. S. Ghyngazov, Russ. Phys. J., **63 (5)**, 894 (2020). DOI https://doi.org/10.1007/s11182-020-02114-3.
18. V. G. Kostishin, R. I. Shakirzyanov, A. G. Nalogin, S. V. Shcherbakov, I. M. Isaev, M. A. Nemirovich, M. A. Mikhailenko, M. V. Korobeinikov, M. P. Mezentseva, and D. V. Salogub, Phys. Solid State, **63 (3)**, 435 (2021). DOI: 10.1134/S1063783421030094.
19. I. M. Isaev, S. V. Shcherbakov, V. G. Kostishin, A. G. Nalogin, V. V. Mokljak, B. K. Ostafijchuk, A. A. Alekseev, V. V. Korovushkin, E. A. Belokon', M. V. Kalinyuk, M. A. Mihaylenko, M. V. Korobeynikov, A. A. Bryazgin, and D. V. Salogub, Russ. Microelectron., **48 (8)**, 531 (2019). DOI:10.1134/S1063739719080079.
20. E. N. Lysenko, V. A. Vlasov, A. P. Surzhikov, S. A. Ghyngazov, Russ. Phys. J., **65 (11)**, 1886 (2023). DOI 10.1007/s11182-023-02847-x